

Intrinsic hole localization mechanism in magnetic semiconductors

H. Raebiger, A. Ayuela[†] and R. M. Nieminen

Laboratory of Physics, Helsinki University of Technology, 02015 HUT, Finland

[†] Donostia International Physics Center (DIPC), 20018 San Sebastian/Donostia, Spain

Abstract. The interplay between clustering and exchange coupling in magnetic semiconductors for the prototype $(\text{Ga}_{1-x}\text{Mn}_x)\text{As}$ is investigated considering manganese concentrations x of 1/16 and 1/32, which are in the interesting experimental range. For $x \sim 6\%$, we study all possible arrangements of two Mn atoms on the Ga sublattice within a large supercell and find the clustering of Mn atoms at nearest-neighbour Ga sites energetically preferred. As shown by analysis of spin density and projected density-of-states, this minimum energy configuration localizes further one hole and reduces the effective charge carrier concentration. Also the exchange coupling constant increases to a value corresponding to lower Mn concentrations with decreasing inter Mn distance.

Including spin information into semiconductor electronics has enormous potential for new applications (see Ref. [1] for a review of magnetoelectronics). Within this field of research, the III-V diluted magnetic semiconductors (DMS) have opened up a new chapter, in particular $(\text{Ga,Mn})\text{As}$ is a prominent candidate for a spintronics material. This compound, grown by means of low-temperature molecular beam epitaxy (LT-MBE), [2–5] shows ferromagnetism [2–8] with a Curie temperature as large as 110 K in the Mn concentration range between 5% and 10% [3–5]. The ferromagnetism (FM) in $(\text{Ga,Mn})\text{As}$ is mediated by holes that are antiferromagnetically (AFM) coupled to the Mn. In spite of the tremendous theoretical effort to explain the interplay of magnetism and semiconductor properties [9–18], a number of fundamental questions still remain unresolved. Such is the so-called hole compensation problem: although the substitutional Mn is a single acceptor and should introduce one hole, the observed hole concentrations are at least an order of magnitude smaller than the Mn concentration [19]. This hole compensation has been ascribed to intrinsic defects such as Mn interstitials [20] and As antisites [12]. However, the antisite concentrations are small, interstitial Mn has a high formation energy compared with substitutional Mn [20,21], and the interstitial Mn has a rather low migration barrier so annealing will reduce interstitial concentrations [22]. Still, after growth condition optimization and thermal annealing the hole compensation cannot completely be eliminated, and long-time annealing reduces further the hole concentration [8]. We focus on the hypothetical defect-free $(\text{Ga}_{1-x}\text{Mn}_x)\text{As}$ and consider hole compensation due to intrinsic properties of the substitutional Mn and the spin-polarized holes, bonding and localization effects.

In this Letter we present first principles calculations for magnetic semiconductors. Within the density-functional theory we test all-electron methods, the full potential linearized augmented plane wave (FLAPW) method [23] and the projector augmented-wave (PAW) method [24, 25], as well as a plane wave pseudopotential (PWPP)

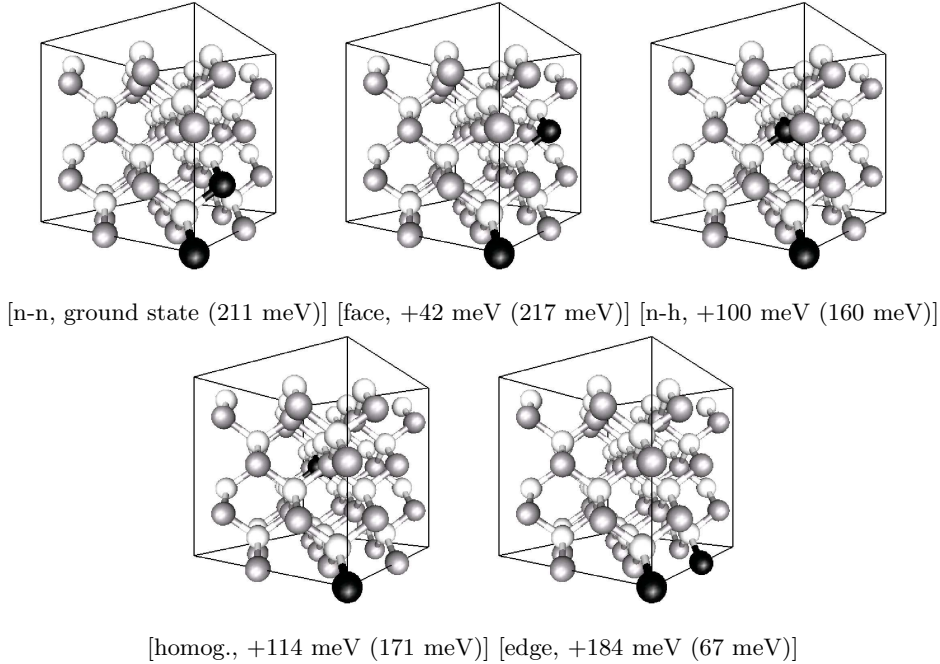


Figure 1. Structures of the $(\text{Ga}_{1-x}\text{Mn}_x)\text{As}$ system with $x \sim 6\%$ and successive stages of clustering. Ga atoms are shown as grey, Mn atoms as black, and As as white. They are ordered according to the energy in meV respect to the ground state, given by the number below the structures. In parenthesis the antiferromagnetic-ferromagnetic AFM-FM energy differences $\Delta_{\text{AFM-FM}}$ are also provided.

method [24]. We also test the generalized gradient approximation (GGA) beyond the local spin density (LSD) approximation [26,27] for the exchange-correlation functional. We then investigate Mn clustering in $(\text{Ga},\text{Mn})\text{As}$ within the supercell approach (see Fig.1 describing the considered cases), which gives us hints as to comment on hole localization. Based on the clustering results, we reexamine the findings of previous calculations that address the role of the exchange coupling parameter within mean-field theories.

As a benchmark we study zincblende MnAs which is a bulk equivalent to the substitutional Mn in GaAs [9,13]. To ensure convergence in energy and magnetic moment with respect to k-points and cutoff parameters, especially the structure of the density-of-states (DOS) was monitored. We see in Table 1 obvious differences between our full-potential and pseudopotential calculations for the lattice constants between GGA and LSD results. They show errors of the order of 0.1 \AA , which are far from negligible because one is near the transition from metallic behaviour to a half-metallic state. Both the lattice constants as well as the electronic behaviour show differences with respect to previous calculations [10,17]. The differences concerning pseudopotential calculations might be ascribed to the used pseudopotentials, while the difference with previous full-potential calculations sounds more puzzling. To correctly observe the metallic or half-metallic behaviour, a denser mesh beyond a typical semiconductor k-point sampling is required. Apart from the intrinsic pseudopotential

Table 1. Equilibrium lattice constant and electronic behaviour for the zincblende MnAs structure. The calculations have been done within several density-functional methods with different treatments: i) for the atom potential (FLAPW- and PAW- full potential; PWPP- pseudopotentials); ii) or for the correlation approximation (GGA- generalized gradient approximation; LSD- local spin density approximation).

	Lattice constant(Å)		equilibrium behaviour	
	GGA	LSD	GGA	LSD
FLAPW	5.63	5.34	metallic	metallic
	-	5.85 [9]	-	half-metal
PWPP	5.72	5.39	half-metal	metallic
	-	5.6-5.7 [13]	-	metallic
PAW	5.61	5.33	metallic	metallic

differences, the k-point consideration remains also as the main difference with respect to previous pseudopotential calculations (see Fig 4 in Ref. [17], where the magnetization shows spurious jumps with the distance). The tests clearly show that calculations must be carried out within all-electron methods and the GGA. The PAW calculations are computationally nearly as efficient as the PWPP ones, so the PAW GGA approach is employed henceforth. We have made simulations of $\text{Ga}_{1-x}\text{Mn}_x\text{As}$ with $x=1, \frac{1}{16},$ and $\frac{1}{32}$ where the notation of x means $\frac{\text{Mn-atoms}}{\text{As-sites}}$ in the supercell. Naturally the size of the supercell is twice the number of As sites. We only consider substitutional Mn in the Ga sublattice, and focus on the clustering process of 2 Mn atoms in the high Curie temperature region of $x \sim 6\%$. Here we include 2 Mn atoms in the 64 atom supercell (*i.e.* $x = \frac{2}{32}$) and calculate all five possible Mn arrangements corresponding to different Mn-Mn distances, as shown in Fig 1. Again we test for convergence with respect to the number of k-points and cutoff parameters: for the 64 atom supercell a 4x4x4 mesh including the Γ point is sufficient to sample the Brillouin zone, and plane waves up to the cutoff of 275 eV give converged results. The lattice atoms are relaxed so that the forces in the system are lower than 0.02 eV/Å.

First we investigate the clustering process of Mn on the Ga sublattice. In Fig. 1 the geometries are ordered according to their energy. The energetic order depends on the Mn-Mn atom distance except for the "edge" configuration. It is interesting to remark that the nearest neighbour configuration has the lowest energy which indicates clustering, as also predicted using the atomic sphere approximation for the potential [15]. This clustering could play a role in the magnetic order. Thus, the energetic differences ΔE_{AFM-FM} between ferromagnetic and antiferromagnetic configurations, *i.e.* two Mn with parallel or antiparallel magnetic moments, are also given in parenthesis in Fig. 1. Tests on larger supercells showed that ΔE_{AFM-FM} is independent of supercell size. The magnetic ground state of all the configurations is ferromagnetic with a magnetic moment of 4 μ_B per Mn atom in the unit cell, as for the homogenous case in Ref [13]. The ΔE_{AFM-FM} values increase when decreasing the Mn-Mn distance. For the edge configuration, the ΔE_{AFM-FM} is considerably smaller than in the other configurations. This configuration constitutes an exception because the As atoms are in a more open structure, which enables direct AFM coupling between the two Mn atoms. Considering the other cases, even for the larger distances, in the homogenous distribution, the values ΔE_{AFM-FM} are large compared with similar materials [28]. When neglecting the barriers involved in the process, the energies

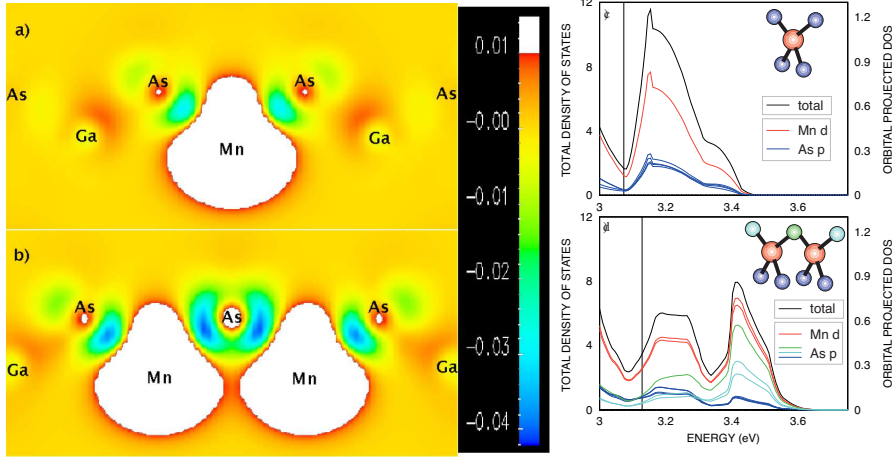


Figure 2. (Color) Spin density $\rho_{\uparrow} - \rho_{\downarrow}$ in the (110) plane around Mn (a and b) and majority spin density of states (c and d) in the n-n and homogeneous case. Units in $\mu_B \text{\AA}^{-3}$. Values over $0.1 \mu_B \text{\AA}^{-3}$ are truncated and given in white color. The DOS are given in states per supercell; black line for total DOS and coloured lines for orbital projected DOS. The red line represents Mn *d* states, the green, turquoise and blue lines represent the As *p* states corresponding to different As sites, as shown in inset.

required by the Mn to jump between different Ga sites are smaller than the energies required to flip the spins. In other words, the growth under strong magnetic fields should affect the final atomic configuration.

Next we focus on the hole localization seen in the spin-density as well as the density of states (DOS), and look for quantifications by integrating over both spin-density and DOS. The spin polarized charge density for the nearest neighbour and homogeneous case is presented in Fig. 2 a and b. The negative spin density in the n-n configuration is more concentrated around the As nuclei than in the homogeneous one, especially around the As atom shared as first neighbour by both Mn atoms. As FM is mediated by holes which are AFM coupled to Mn atoms, the negative spin density points out the hole density. Therefore this localization of negative spin density implies that the holes undergo strong localization in the n-n case.

This dimer-induced hole localization is further clarified in the DOS shown in Fig. 2 c and d, where the t_d -like hole states split into bonding and antibonding states. Since we are discussing hole states, the behaviour is opposite to electronic states, i.e. the bonding-like hole states are higher in energy (deeper in the gap, larger effective mass and higher localization). From the orbital projected DOS (PDOS) we observe that the As *p* states around the in-between-As (green curve) provide a significant contribution to the DOS in the unoccupied region. In homogeneous case the unoccupied states correspond to antibonding t^a states that account for the Mn induced itinerant hole states responsible for ferromagnetism (see Ref. [29]). In the n-n configuration, the t_d symmetry break splits the t^a state into an antibonding state and a bonding like state deeper in the gap. The deeper state, according to PDOS analysis, is localized around the in-between-As, and therefore we are left only with one itinerant t^a like hole state, reducing the effective carrier concentration by one half.

For a quantitative measure of how the holes are distributed on atomic orbitals we integrate the PDOS over the unoccupied valence band states; the absolute values depend on the basis set used, projection details etc., but relative values provide useful information when comparing different systems. In the dimer configuration we observe 0.1, 0.05 and 0.03 unoccupied p states on the in-between-As (green), the end-As (turquoise) and the vertical-As (blue), respectively following notation in Fig. 2. In case of the homogeneous distribution, we observe 0.04 unoccupied p states on the As next to Mn. It is interesting to compare the integrated hole densities with magnetization around As (*i.e.* spin-density integrated inside sphere): In the dimer configuration we observe values of $-0.077 \mu_B$, $-0.032 \mu_B$ and $-0.009 \mu_B$ around the in-between-As, end-As and vertical-As, respectively, while in the homogeneous case the magnetization of the As next to Mn is $-0.025 \mu_B$. The similar values for unoccupied As p states and As magnetization confirm that the negative spin-density actually is correlated with the hole density. Notice that both values on the in-between-As get over twice the ones in the homogeneous case, which is a non-negligible quantity. Thus this hole localization mechanism seen both in spin density and DOS, combined with the lowered energy in the n-n configuration is a significant addition to the previously known mechanisms that reduce the effective carrier concentration. With this finding we give a possible explanation why only a fraction of the Mn align ferromagnetically and why a large number of holes is lost, even when we are limited to only Mn in substitutional positions.

The change of DOS and the charge polarization for the different configurations drives us to address the same issues for the exchange coupling parameter $N\beta$, which is crucial in the calculation of thermodynamic properties [18]. Following Ref. [13], the effect of the sp-d exchange on the band structure of the host semiconductor can be related with the spin splitting at the gamma point. Although both conduction as well as valence band splitting can be considered, we concentrate only on the $N\beta$ parameter because it shows largest changes with the inclusion of magnetism. The valence exchange coupling constant can be written as

$$N\beta = \frac{\Delta E^v}{x \cdot \langle S \rangle},$$

where ΔE^v is the valence band edge spin splitting at the Γ point, and the mean field spin $\langle S \rangle$ is half of the computed magnetization per Mn ion. Experimentally this constant is extracted from the exciton band that is spin split in optical magnetoabsorption experiments. Our estimated exchange couplings are given in Fig. 3.

The parameter $N\beta$ for both concentrations shows values between 5.6-6.8 eV. With respect to previous PWPP results, 5.48 eV for $x=1/16$ and 7.34 eV for $x=1/32$ [13], $N\beta$ does not depend strongly on the Mn concentration. For the concentration $x = 2/32$ the $N\beta$ parameter for several Mn configurations increases as the longest distance between Mn atoms increases. Its value approaches that of the smaller concentration $x=1/32$. It seems that the longest Mn-Mn distance sets the exchange over the whole semiconductor. A simple mean-field model might after all be justified when re-interpreting the exchange constant in terms of holes ascribed both to Mn as well as Mn dimers, *i.e.* the Mn dimer should be treated like a single Mn impurity. This is because the exchange is mediated by the itinerant holes, and as seen in Fig. 2 d, in the n-n case the two Mn as a total contribute only one t^a like itinerant hole. All these findings suggest that the breakdown of the mean field approximation is not yet

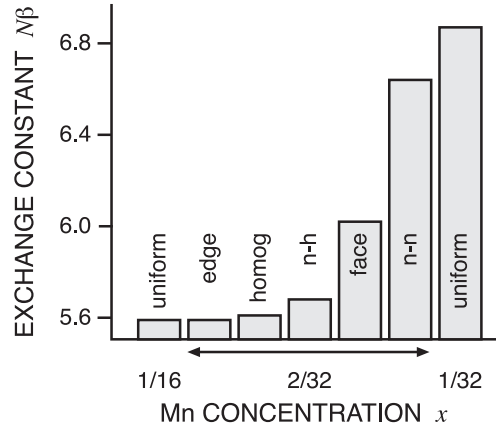


Figure 3. Exchange constant $N\beta$ (in eV) as a function of the Mn concentration x . Also they are given as a function of the geometrical arrangement for the Mn concentration $x=2/32$.

well established, *i.e.* a mean field scheme may be justified by including this clustering process.

In conclusion, we see that disorder has strong effect on the ferromagnetic coupling. The preferred structural configuration is a dimer of two Mn occupying nearest neighbour Ga sites. This configuration localizes a hole and explains in part the reduced carrier concentration observed in experiments. Further, our results suggest that the analysis of the breakdown in the mean field approximation should be reconsidered.

Acknowledgments

This work has been supported by the Academy of Finland (Centers of Excellence Program 2000-2005). A. Ayuela is supported by the EU TMR program (Contract No. ERB4001GT954586). Computer facilities of the Center for Scientific Computing (CSC) Finland are greatly acknowledged. We thank K. Saarinen, K. Sato, H. Katayama-Yoshida, J. von Boehm, M. J. Puska and M. Perez-Jigato for discussions during this work.

References

- [1] G. Prinz 1998 *Science* **282** 1660
- [2] H. Munekata, H. Ohno, S. von Molnar, Arin Segenmüller, L. L. Chang and L. Esaki 1989 *Phys. Rev. Lett.* **63** 1849
- [3] H. Ohno 1998 *Science* **281** 951
- [4] H. Ohno and F. Matsukura 2001 *Solid State Communications* **117** 179
- [5] H. Ohno 1999 *J. Magn. Magn. Mater* **200** 110
- [6] H. Ohldag, V. Solinus, F. U. Hillebrecht, J. B. Goedkoop, M. Finazzi, F. Matsukura and H. Ohno 2000 *Appl. Phys. Lett.* **76** 2928
- [7] T. Hayashi, Y. Hashimoto, S. Katsumoto and Y. Iye 2001 *Appl. Phys. Lett.* **78** 1691
- [8] S. J. Potashnik, K. C. Ku, S. H. Chun, J. J. Berry, N. Samarath and P. Schiffer 2001 *Appl. Phys. Lett.* **79** 3493
- [9] M. Shirai 2001 *Physica E* **10** 143
- [10] M. Shirai, T. Ogawa, I. Kitagawa and N. Suzuki 1998 *J. Magn. Magn. Mater.* **177-181** 1383
- [11] T. Ogawa, M. Shirai, N. Suzuki and I. Kitagawa 1999 *J. Magn. Magn. Mater.* **196-197** 428

- [12] H. Akai 1998 *Phys. Rev. Lett.* **81** 3002
- [13] S. Sanvito, P. Ordejón and N. A. Hill 2001 *Phys. Rev. B* **63** 165206
- [14] J. Inoue, S. Nonoyama and H. Itoh 2000 *Phys. Rev. Lett.* **85** 4610
- [15] M. van Schilfgaarde and O. N. Mryasov 2001 *Phys. Rev. B* **63** 233205
- [16] S. Sanvito and N. A. Hill 2001 *Appl. Phys. Lett.* **78** 3493
- [17] S. Sanvito and N. A. Hill 2000 *Phys. Rev. B* **62** 15553
- [18] J. König, J. Schliemann, T. Jungwirth and A. H. MacDonald *cond-mat/0111314*
- [19] T. Slupinski, H. Munekata and A. Oiwa 2002 *Appl. Phys. Lett.* **80** 1592
- [20] S.C. Erwin and A.G. Petukhov 2002 *Phys. Rev. Lett.* **89** 227201
- [21] P. Mahadevan and A. Zunger *cond-mat/0309502*
- [22] K. W. Edmonds, P. Boguslawski, K. Y. Yang, R. P. Campion, S. N. Novikov, N. R. S. Farley, B. I. Gallagher, C. T. Foxton, M. Sawicki, T. Dietl, M. Buongiorno Nardelli and J. Bernhole 2004 *Phys. Rev. Lett* **92** 37201
- [23] P. Blaha, K. Schwarz and J. Luitz, WIEN97, Vienna University of Technology, 1997, (An improved and updated Unix version of the copyrighted WIEN-code (P. Blaha, K. Schwarz, P. Sorantin and S.B. Trickey 1990 *Comput. Phys. Commun.* **59** 399).
- [24] G. Kresse and J. Furthmüller 1996 *Phys. Rev. B* **54** 11169; G. KRESSE AND J. FURTHMÜLLER, *VASP the Guide* (Vienna University of Technology, Vienna, 1999) [<http://tph.tuwien.ac.at/~vasp/guide/vasp.html>].
- [25] G. Kresse and D. Joubert 1990 *Phys. Rev. B* **41** 5414
- [26] J.P. Perdew, J.A. Vosko, S.H. Vosko, K.A. Jackson, M.R. Pederson, D.J. Singh and C. Fiolhais 1992 *Phys. Rev. B* **46** 6671
- [27] J.P. Perdew and Y. Wang 1992 *Phys. Rev. B* **45** 13244; and references therein.
- [28] B. Sanyal, O. Bengone and S. Mirbt 2003 *Phys. Rev. B* **68** 205210
- [29] K. Sato, P.H. Dederichs, and H. Katayama-Yoshida 2003 *Europhys. Lett.* **61** 403